JOURNAL OF AIRCRAFT
Vol. 36, No. 1, January–February 1999

Aeroelastic Loads and Sensitivity Analysis for Structural Loads Optimization

R. D'Vari* and M. Baker†
The Boeing Company, Long Beach, California 90807

An aeroelastic integrated loads subsystem (AILS) is being developed and verified for the calculation of aeroelastic loads for analysis and design. AILS will fit within the aeroelastic design optimization program. The purpose of AILS is to integrate the maneuver and gust loads calculation process with structural analysis and optimization. AILS' active control capabilities and analytical sensitivity analysis will allow a simultaneous optimization of loads, structures, and active load alleviation system with flutter and other aeroelastic constraints. This first version of AILS includes a linear analysis for steady maneuver and unsteady aeroservoelastic gust loads and their sensitivities to structural design variables and control parameters. AILS static aeroelastic analysis offers 1) full aircraft aeroelastic trim using aircraft angles of attack and sideslip, control-surface deflections, and/or motion rates and accelerations; 2) balanced distributed aeroelastic loads; 3) stress-based critical loads selection; 4) wing jig shape calculations for a specified nominal cruise wing shape and loading; 5) static aeroelastic stability and control derivatives and control effectiveness; and 6) static aeroelastic load sensitivities to structural design variables with constrained or variable nominal cruise shape to be used in optimization. The aeroservoelastic gust load capabilities in AILS include 1) random frequency response analysis for displacement, velocity, acceleration, element force, and stress; 2) flight control and active load alleviation system; 3) calculation of rms and zero-crossing frequency; and 4) analytical derivative of random gust response to control gains. These analyses are compared with MSC/NASTRAN and a proprietary dynamic analysis program (C4EZ). The results of comparisons for the static aeroelastic and gust response analyses of AILS are shown for two commercial transport aircraft: one is a wide-body subsonic transport and the other is a high-speed civil transport configuration at subsonic conditions. The static loads and stability derivatives for two models are compared with MSC/NASTRAN for both aircraft, and gust loads are compared with a production gust-load analysis for the subsonic transport case. In all cases excellent agreement is obtained. Validation of AILS' load sensitivity calculations was done through comparison with the finite difference approach. Excellent agreement was obtained between analytical and numerical derivatives.

Nomenclature

$[\mathrm{AIC}^c]$ = theoretical aerodynamic influence coefficient matrix (e.g., doublet-lattice, doublet-point, or harmonic gradient), corrected to match experimental or computational fluid dynamics data
$[B_{ij}]$ = feedback control laws relating the commanded control surface motion $\{u_x\}$ to the aircraft response in the frequency domain
$\{F^g\}$ = generalized gust column in a doublet aerodynamic analysis, which is the vector of rigid aerodynamic forces generated in response to a unit traveling sinusoidal gust at a given wavelength for a unit dynamic pressure
$[K_{xx}]$ = control actuator stiffness
k = reduced frequency, $\omega c/2V_\infty$
$[M_{lr}]$ = generalized rigid-body mass matrix with respect to elastic modes (a zero matrix for orthogonal elastic modes)
$[M_{rr}]$ = generalized mass matrix for the rigid-body degrees of freedom
$\{\bar{P}^a_{A_{C0\text{-}g}}\}$ = vector of aerodynamic twist and camber forces for the jig shape (0-g) wing shape at zero α per unit dynamic pressure
$[\mathrm{PPM}_{sa}]$ = panel-pointing matrix for aerodynamic forces
$[\mathrm{SPM}_{as}]$ = matrix that splines the displacements in the structural coordinate system to the aerodynamic coordinate system
$\{u^a_l\}$ = aeroelastic deflections in the aerodynamic coordinate system
$\{u_x\}$ = aerodynamic trim variables, includes angles of attack and sideslip, control-surface deflections, and/or motion rates
$\{\eta_c\}$ = frequency response of rigid control-surface modes
$\{\eta_l\}$ = modal elastic degrees of freedom
$\{\eta_r\}$ = frequency response of the generalized rigid aircraft modes
$\{\ddot{\eta}_r\}$ = aircraft steady rigid-body translational and rotational accelerations
$[\phi^a_l]$ = matrix of structural modes in the aerodynamic coordinate system
$[\phi^s_l]$ = matrix of structural modes in the structural coordinate system

Received Dec. 3, 1997; revision received April 1, 1998; accepted for publication Aug. 9, 1998.

*Principal Engineer Scientist; currently Vice President and Head of Quantitative Analysis, State Street Research & Management, Boston, MA 02111. Associate Fellow AIAA.
†Senior Engineer. Member AIAA.

Introduction

EFFICIENT and reliable design of modern aircraft requires accurate and timely predictions of aeroelastic maneuver and gust loads for numerous conditions. The trend in aircraft design has been to use simultaneous strength/flutter optimization along with detailed finite element models (FEMs), and so it is required that an industrial loads system work with FEM

structural models and fit into a larger optimization framework. Most formal optimization or fully stressed designs are performed under fixed loading conditions and neglect all or part of the change of aeroelastic loads caused by design variable changes. This approach neglects a potential reduction of loads through passive load alleviation. The introduction of load sensitivities to structural design variables and the sensitivities of stresses to load changes in the optimization process can lead to true aeroelastic tailoring and, hence, lighter structures.

One important step in the accurate calculation of loads and their sensitivities is in the calculation of the jig shape. In general, the wing shape at a nominal cruise condition is specified by the aerodynamic considerations, viz., lift-to-drag ratio, $C_{L_{max}}$, pitch up, etc. Generally, the wing jig shape (0-g shape in vacuum) is devised in such a way to achieve the proper shape during the cruise condition, and it depends on the wing structural stiffness. In calculating load sensitivities, both aircraft trim and jig shape changes must be accounted for.

Further load reductions and weight savings can be achieved through control surfaces such as spoilers and ailerons, and future fuel-efficient large-transport aircraft will utilize such control surfaces as load-alleviation devices. In the design of active wing load alleviation systems, it is necessary compute loads and their sensitivities, including the effects of control-system parameters.

In this study, the first release of an aeroelastic integrated loads subsystem (AILS[1]) has been developed, based on a finite element representation of the free-flying aircraft and an aerodynamic influence coefficient (AIC) representation of the steady and unsteady aerodynamics. The results presented here are limited to doublet-lattice subsonic aerodynamics.[2,3] AILS is being implemented and verified within a large-scale aeroelastic design optimization program (ADOP).[4,5] ADOP has two separate sizing procedures: 1) fully stressed design for strength and 2) numerical multidisciplinary optimization for static strength and displacement, flutter, and modal frequency. ADOP allows multiple load cases, automatic buckling and damage tolerance allowable stress calculations, and manufacturing constraints on the design variables. Simultaneous strength and flutter optimization can be performed using multiple load cases and flight envelope data. For the numerical multidisciplinary optimization sizing approach, ADOP uses the method of modified feasible directions in the DOT optimization code.[6] Recent full aircraft optimization studies involving ADOP include the strength optimization of high-speed civil transport (HSCT)[7] shown in Fig. 1, and a simultaneous strength/flutter optimization of a wide-body subsonic transport.[8] Figure 2 shows the role of AILS within ADOP. AILS has both static and dynamic analysis functions, and provides 1) trimmed distributed static aeroelastic loads, 2) design gust loads including aeroservoelastic effects, 3) maneuver and gust load alleviation, and 4) aeroservoelastic load sensitivities to structural and control design variables.

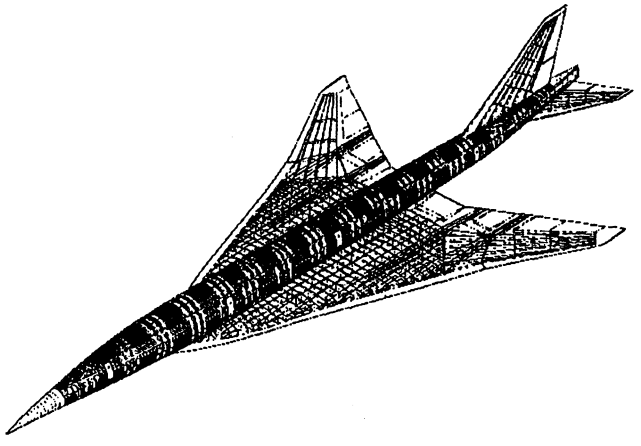

Fig. 1 HSCT test case structural CAD model.

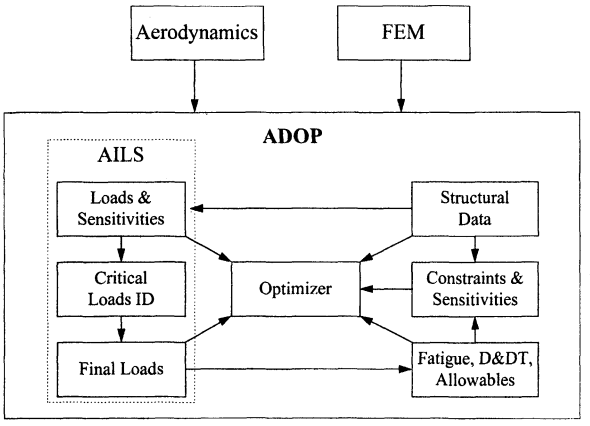

Fig. 2 AILS in ADOP.

Static Aeroelasticity

The AILS formulation for aeroelastic trim is based on a modal approach, using FEM-based normal modes for the free-flying aircraft. It is assumed that the structure behaves linearly, and that the aerodynamics are quasisteady, i.e., zero reduced frequency, and linearized such that the aerodynamic forces can be represented as an AIC matrix plus a basic pressure distribution vector. Currently, AILS uses subsonic doublet-lattice aerodynamics, and some candidate supersonic methods are ZONA,[9,10] Woodward,[11] and the doublet-point method.[12] A procedure for correcting linear aerodynamics based on experimental or computational fluid dynamics (CFD) data is available,[13,14] in which the linear aerodynamic influence coefficient matrix is updated based on equivalent values of a local aerodynamic coefficient. The aeroelastic equilibrium equations, balance equations, and trim variable constraint equations are solved simultaneously for the elastic displacements, aircraft attitude, and control-surface deflections, and other trim variables such as rigid-body motion rates.

Aerodynamic Loads

The experimentally corrected aerodynamic forces caused by elastic deflections (expressed in the aerodynamic coordinate system), aerodynamic trim variables, and the aircraft camber and twist at zero angle of attack (α), are given by

$$\{F_A^s\} = \bar{q}_{\text{dyn}}[\text{PPM}_{sa}]\{[\text{AIC}^C]\{\{u_l^a\} + [\phi_x^a]\{u_x\}\} + \{\bar{P}^a_{A_{C0\text{-}g}}\}\} \tag{1}$$

The aerodynamic displacement vector as a result of the elastic deflections can be further expanded into

$$\{u_l^a\} = [\text{SPM}_{as}]\{u_l\} = [\text{SPM}_{as}][\phi_l^s]\{\eta_l\} = [\phi_l^a]\{\eta_l\} \tag{2}$$

An important feature in an aeroelastic solution method is the coupling between aerodynamic and structural models. In AILS, this is accomplished through the splining matrix $[\text{SPM}_{as}]$, which converts structural deflections in the FEM coordinate system to deflections of the aerodynamic model in an aerodynamic coordinate system, and the panel-pointing matrix $[\text{PPM}_{sa}]$, which converts pressures on the aerodynamic model into equivalent FEM nodal forces. The MSC/NASTRAN aeroelastic solutions and, currently, AILS use a fairly abstract virtual work principle that leads $[\text{PPM}_{sa}]$ to be the same as the transpose of the displacement spline matrix. However, this can sometimes lead to unreasonable patterns of distributed loads in the structural system, and a robust method of converting loads from aerodynamic degrees of freedom to the structural

degrees of freedom is being developed in AILS that is based on a more physical concept. However, all of the results presented in this paper are based on the virtual work principle. $[\mathrm{SPM}_{as}]$ is computed using the available spline options in ADOP, i.e., Harder and Desmarais,[15] motion axis, and motion point spline procedures. The Harder and Desmarais spline is used for flexible surfaces, motion axis is used for beam-type structures, and motion point is used for rigid bodies attached to aircraft such as a nacelle.

Equation (1) can be rewritten in a symbolic form as

$$\{F_A^a\} = -[K_{ll}^a]\{u_l\} - [K_{lx}^a]\{u_x\} + \{F_{A_{C0\cdot g}}^s\} \tag{3}$$

where the aerodynamic stiffness matrices and jig loads in the direct degrees of freedom are

$$[K_{ll}^a] = -\bar{q}_{\mathrm{dyn}}[\mathrm{PPM}_{sa}][\mathrm{AIC}^C][\mathrm{SPM}_{as}] \tag{4}$$

$$[K_{lx}^a] = -\bar{q}_{\mathrm{dyn}}[\mathrm{PPM}_{sa}][\mathrm{AIC}^C][\phi_x^a] \tag{5}$$

$$\{F_{A_{C0\cdot g}}^s\} = \bar{q}_{\mathrm{dyn}}[\mathrm{PPM}]\{\bar{P}_{A_{C0\cdot g}}^a\} \tag{6}$$

The aerodynamic loads in the modal form can be expressed as

$$\{F_A\} = [\phi^s]^T\{F_A^s\} \tag{7}$$

The elastic and rigid generalized forces are

$$\begin{aligned}\{F_{A_l}\} &= -[\mathcal{H}_{ll}^a]^T\{\eta_l\} - [\mathcal{H}_{lx}^a]^T\{u_x\} + \{\mathcal{P}_{A_{cl}}^{0\cdot g}\}\\ \{F_{A_r}\} &= -[\mathcal{H}_{rl}^a]^T\{\eta_l\} - [\mathcal{H}_{rx}^a]^T\{u_x\} + \{\mathcal{P}_{A_{cr}}^{0\cdot g}\}\end{aligned} \tag{8}$$

where the various modal aerodynamic stiffnesses are given by

$$[\mathcal{H}_{ll}^a] = -\bar{q}_{\mathrm{dyn}}[\phi_l^s]^T[\mathrm{PPM}_{sa}][\mathrm{AIC}^C][\mathrm{SPM}_{as}][\phi_l^s] \tag{9}$$

$$[\mathcal{H}_{lx}^a] = -\bar{q}_{\mathrm{dyn}}[\phi_l^s]^T[\mathrm{PPM}_{sa}][\mathrm{AIC}^C][\phi_x^a] \tag{10}$$

$$[\mathcal{H}_{rl}^a] = -\bar{q}_{\mathrm{dyn}}[\phi_r^s]^T[\mathrm{PPM}_{sa}][\mathrm{AIC}^C][\mathrm{SPM}_{as}][\phi_l^s] \tag{11}$$

$$[\mathcal{H}_{rx}^a] = -\bar{q}_{\mathrm{dyn}}[\phi_r^s]^T[\mathrm{PPM}_{sa}][\mathrm{AIC}^C][\phi_x^a] \tag{12}$$

and the generalized jig loads are given by

$$\{\mathcal{P}_{A_{cl}}^{0\cdot g}\} = [\phi_l^s]^T\{F_{A_{C0\cdot g}}^s\}, \qquad \{\mathcal{P}_{A_{cr}}^{0\cdot g}\} = [\phi_r^s]^T\{F_{A_{C0\cdot g}}^s\} \tag{13}$$

Static Aeroelastic Equations

With the definitions of the previous section, the equilibrium equations for the generalized elastic and rigid-body degrees of freedom can be written as

$$\begin{aligned}[\mathcal{H}_{ll}]\{\eta_l\} &= \{\mathcal{F}_{I_l}\} + \{\mathcal{F}_{A_l}\}\\ &= -[\mathcal{M}_{lr}]\{\ddot{\eta}_r\} - [\mathcal{H}_{ll}^a]\{\eta_l\} - [\mathcal{H}_{lx}^a]\{u_x\} + \{\mathcal{P}_{A_{cl}}^{0\cdot g}\}\end{aligned} \tag{14}$$

$$\begin{aligned}\{0\} &= \{\mathcal{F}_{I_l}\} + \{\mathcal{F}_{A_l}\}\\ &= -[\mathcal{M}_{rr}]\{\ddot{\eta}_r\} - [\mathcal{H}_{rl}^a]\{\eta_l\} - [\mathcal{H}_{rx}^a]\{u_x\} + \{\mathcal{P}_{A_{cr}}^{0\cdot g}\}\end{aligned} \tag{15}$$

Equation (14) represents the elastic equilibrium equations of the flexible aircraft, and Eq. (15) represents the balance (rigid-body equilibrium) equations for the total aircraft. This is an underdetermined set of equations and must be augmented with additional equations to define the maneuver condition. AILS uses a single matrix equation to serve several purposes in connection to the specification of any general trim conditions, relations, or active control laws. This common form is given by

$$[\mathcal{B}_{xl}\ \mathcal{B}_{xr}\ \mathcal{B}_{xx}]\begin{Bmatrix}\eta_l\\ \ddot{\eta}_r\\ u_x\end{Bmatrix} = \{\mathcal{C}_x\} \tag{16}$$

The $[B_{xl}]$, $[B_{xr}]$, $[B_{xx}]$, and $\{C_x\}$ matrices can be specified by the user to enforce any combination of 1) specification of fixed settings for the control surfaces, trim variables, or aircraft load factors; 2) specification of a set of control relations for the steady maneuver load alleviation; and 3) a set of preprogrammed linear relationships among various control-surface deflections. Equation (16) is flexible enough to accommodate any form of linear control laws for quasisteady maneuvers. This form also makes the formulation and implementation of the balanced aeroelastic loads sensitivities that include active control laws very tractable and procedurally simple. Equations (14–16) can conveniently handle, in the future, any nonlinear aerodynamic representation or control relationship through an iterative quasilinearization procedure. These equations can be collected to express the overall steady maneuver equations of motion for a free–free aircraft:

$$\begin{bmatrix}\mathcal{H}_{ll} + \mathcal{H}_{ll}^a & \mathcal{M}_{lr} & \mathcal{H}_{lx}^a\\ \mathcal{H}_{rl}^a & \mathcal{M}_{rr} & \mathcal{H}_{rx}^a\\ \mathcal{B}_{xl} & \mathcal{B}_{xr} & \mathcal{B}_{xx}\end{bmatrix}\begin{Bmatrix}\eta_l\\ \ddot{\eta}_r\\ u_x\end{Bmatrix} = \begin{Bmatrix}\mathcal{P}_{A_{cl}}^{0\cdot g}\\ \mathcal{P}_{A_{cr}}^{0\cdot g}\\ \mathcal{C}_x\end{Bmatrix} \tag{17}$$

Two comments on Eq. (17) are in order. First, if the mode shapes used in the solution are free–free orthogonal modes, then the trim equations are implicitly expressed in terms of a mean axis. Second, the number of aerodynamic trim variable, n_x, can be larger than the number of the free rigid degrees of freedom to be balanced, n_r, but must come after the following relationship:

$$n_x = n_r + n_c \tag{18}$$

i.e., the total number of aerodynamic trim variables, n_x, must be equal to the sum of the number of rigid-body equilibrium equations, n_r, and the number of enforced control relations, n_c. Note that n_c includes all fixed values of control-surface deflections and load factors, control schedules, and control laws. To solve the trim [Eq. (17)], aerodynamic loads for the jig shape are required, i.e., $\mathcal{P}_{A_{cl}}^{0\cdot g}$ and $\mathcal{P}_{A_{cr}}^{0\cdot g}$. The solution for the jig loads are discussed next.

Solution of Jig Loads

Typically, the nominal cruise shape (twist and camber) of an aircraft is dictated by aerodynamic performance considerations. This cruise shape is, by definition, an elastically deformed shape resulting from the 1-g cruise loads. The aeroelastic equilibrium equations, on the other hand, require a definition of the aerodynamic loads on the undeformed, i.e., as-built or jig, airplane. To solve the quasisteady maneuver [Eq. (17)], the jig shape and corresponding loads must be first calculated from the nominal cruise condition.

The jig shape calculation procedure is considerably simplified by the fact that the cruise shape is known a priori. The problem is determining a combination of elastic deflection and undeformed shapes that results in the correct cruise shape. Because the aerodynamic loads (which are a function of the cruise shape), are also known a priori, the elastic deflection can be easily computed, and the jig shape inferred from the cruise shape and elastic deflection. The aerodynamic loads in

the structural degrees of freedom for a nominal cruise condition are given by

$$\{F^s_{A_{1\text{-}g}}\} = \bar{q}_{\text{dyn}_{1\text{-}g}}[\text{PPM}_{sa}][\text{AIC}^C][\phi^a_x]\{u_{x_{1\text{-}g}}\} + \{F^s_{A_{C1\text{-}g}}\} \quad (19)$$

where

$$\{F^s_{A_{C1\text{-}g}}\} = \bar{q}_{\text{dyn}_{1\text{-}g}}[\text{PPM}_{sa}]\{P^a_{A_{C1\text{-}g}}\} \quad (20)$$

is the aerodynamic force (in structural degrees of freedom) on the airplane of nominal cruise shape at zero incidence (trim) variables, i.e., zero angle of attack and control-surface deflection. Note that the cruise airloads are not functions of the elastic deflection, because this is implicitly taken into account in the cruise shape. The generalized 1-g camber and twist loads are given by

$$\{\mathcal{P}^{1\text{-}g}_{A_{C_l}}\} = [\phi^s_l]^T\{F^s_{A_{C_{1\text{-}g}}}\} \quad (21)$$

$$\{\mathcal{P}^{1\text{-}g}_{A_{C_r}}\} = [\phi^s_r]^T\{F^s_{A_{C_{1\text{-}g}}}\} \quad (22)$$

Through a derivation similar to that used for the quasi-steady maneuver case, it can be shown that the jig shape analysis problem can be cast into a single matrix equation:

$$\begin{bmatrix} \mathcal{K}_{ll} & \mathcal{M}_{lr} & \mathcal{K}^a_{lx} \\ 0 & \mathcal{M}_{rr} & \mathcal{K}^a_{rx} \\ \mathcal{B}_{xl} & \mathcal{B}_{xr} & \mathcal{B}_{xx} \end{bmatrix} \begin{Bmatrix} \eta_{l_{1\text{-}g}} \\ \ddot{\eta}_{r_{1\text{-}g}} \\ u_{x_{1\text{-}g}} \end{Bmatrix} = \begin{Bmatrix} \mathcal{P}^{0\text{-}g}_{A_{cl}} \\ \mathcal{P}^{0\text{-}g}_{A_{cr}} \\ \mathcal{C}_x \end{Bmatrix} \quad (23)$$

where the coefficients of the last row of equations are chosen to reflect the definition of the nominal cruise condition. Note that Eq. (23) is very similar to Eq. (17), but that the terms accounting for aerodynamic loads induced by elastic deflection are not present. To compute the jig loads for subsequent maneuver analysis, this equation must be solved for the generalized elastic deflections at the cruise condition $\{\eta_{l_{1\text{-}g}}\}$. Once this piece of information is available, the jig loads for an arbitrary maneuver condition can be computed as

$$\{F^s_{A_{C0\text{-}g}}(M)\} = \{F^s_{A_{C1\text{-}g}}(M)\} - \bar{q}_{\text{dyn}}[\text{PPM}_{sa}][\text{AIC}^C(M)][\phi^a_l]\{\eta_{l_{1\text{-}g}}\} \quad (24)$$

Note that the corrected AIC matrix and the basic airload distribution $\{F^s_{A_{C1\text{-}g}}(M)\}$ on the 1-g cruise shape in Eq. (24) are for the Mach number at which the maneuver analysis is being conducted, *not* at the cruise condition. The explicit dependence of these quantities is included for clarity. Equation (24) can be substituted into Eq. (13) to compute the appropriate terms in Eq. (17) for maneuver solution.

Direct Internal Loads

While the free-vibration modes of an airplane are sufficiently accurate to compute aeroelastic deflections and the corresponding external load distribution, the modal solution is not accurate enough to calculate internal loads and stresses. A summation of force methods is used to calculate a refined estimate of deflections and accurate internal loads and stresses. In this approach, the modal aeroelastic deflections are first used to calculate the external inertial and aerodynamic loads in the direct FEM degrees of freedom. These aeroelastic loads are fully balanced and are then used in a direct static analysis (rather than a modal solution). Once the aeroelastic equations of motion are solved [Eq. (17)], the direct aerodynamic forces are calculated from Eq. (1). The inertia forces are needed for the direct solution, which are given by

$$\{F_I\} = -[M][\phi^s_r]\{\ddot{\eta}_r\} \quad (25)$$

The direct displacements are solved for by ADOP using

$$[K]\{u\} = \{F^s_A\} + \{F_I\} \quad (26)$$

In the preceding equations, $[K]$ and $[M]$ are the direct mass and stiffness matrices. The stiffness matrix $[K]$ is singular for a free–free aircraft. However, because the applied loads are balanced, and the main goal of the direct solution step is to recover accurate FEM deflections and stresses, the direct solution need not be computed on a free–free aircraft. In practice, a suitable boundary condition is specified such that $[K]$ is nonsingular.

Stability Derivatives

To avoid control power deficiency, reversal, and divergence, the stability derivatives are generally constrained in a multidisciplinary optimization design process. The solution for the stability derivatives are given in this section.

Taking the derivative of Eq. (14) with respect to the trim variables, $\{u_x\}$ results in

$$\frac{\partial\{\eta_l\}}{\partial\{u_x\}} = -[\mathcal{K}_{ll} + \mathcal{K}^a_{ll}]^{-1}\left([\mathcal{M}_{lr}]\frac{\partial\{\ddot{\eta}_r\}}{\partial\{u_x\}} + [\mathcal{K}^a_{lx}]\right) \quad (27)$$

Denote

$$[\hat{\mathcal{M}}_{rr}] = [\mathcal{M}_{rr}] - [\mathcal{K}^a_{rl}][\mathcal{K}_{ll} + \mathcal{K}^a_{ll}]^{-1}[\mathcal{M}_{lr}] \quad (28)$$

Taking the derivative of Eq. (15) and substituting from Eq. (28) yields

$$\frac{\partial\{\ddot{\eta}_r\}}{\partial\{u_x\}} = [\hat{\mathcal{M}}_{rr}]^{-1}([\mathcal{K}^a_{rl}][\mathcal{K}_{ll} + \mathcal{K}^a_{ll}]^{-1}[\mathcal{K}^a_{lx}] - [\mathcal{K}^a_{rx}]) \quad (29)$$

$$\frac{\partial\{\mathcal{F}_{A_r}\}}{\partial\{u_x\}} = [\mathcal{M}_{rr}][\hat{\mathcal{M}}_{rr}]^{-1}([\mathcal{K}^a_{rl}][\mathcal{K}_{ll} + \mathcal{K}^a_{ll}]^{-1}[\mathcal{K}^a_{lx}] - [\mathcal{K}^a_{rx}]) \quad (30)$$

The individual derivative terms are defined by

$$SC_{ij} = \frac{1}{\bar{q}_{\text{dyn}}}\frac{1}{A_{x_i}}\frac{\partial\mathcal{F}_{A_{r_i}}}{\partial u_{x_j}} \quad (31)$$

The matrix of stability derivatives $[SC]$ is given by

$$[SC] = \frac{1}{\bar{q}_{\text{dyn}}}\left[\frac{1}{A_x}\right][\mathcal{M}_{rr}][\hat{\mathcal{M}}_{rr}]^{-1}([\mathcal{K}^a_{rl}][\mathcal{K}_{ll} + \mathcal{K}^a_{ll}]^{-1}[\mathcal{K}^a_{lx}] - [\mathcal{K}^a_{rx}]) \quad (32)$$

The $[SC]$ matrix has the dimensions of n_r by n_x. The inertia derivatives can also be derived in a similar fashion. Static aeroelastic derivatives and control effectiveness are calculated for both restrained and unrestrained conditions, depending on the types of modes used (free–free or cantilevered). To avoid calculating restrained modes (in addition to the free–free modes required for the loads analysis), a procedure has been developed and verified in AILS to compute the restrained derivatives using free–free modes.

Static Aeroelastic Load Sensitivities

The load sensitivities to design variables are required for strength optimization. The loads change with design variables in three ways: 1) stiffness and mass changes, 2) trim variable changes, and 3) jig shape changes. A change in stiffness and mass causes both trim variable and jig shape changes. AILS uses an analytical derivative approach that properly accounts

for all three effects. ADOP uses the load sensitivities in determining the displacement and stress constraint sensitivities.

The sensitivity of the aeroelastic solution for a given maneuver is calculated by differentiating the trim equation [Eq. (17)] to get

$$\frac{\partial}{\partial D}\begin{Bmatrix}\eta_l\\ \ddot{\eta}_r\\ u_x\end{Bmatrix} = \begin{bmatrix}\mathcal{K}_{ll}+\mathcal{K}^a_{ll} & \mathcal{M}_{lr} & \mathcal{K}^a_{lx}\\ \mathcal{K}^a_{rl} & \mathcal{M}_{rr} & \mathcal{K}^a_{rx}\\ \mathcal{B}_{xl} & \mathcal{B}_{xr} & \mathcal{B}_{xx}\end{bmatrix}^{-1} \times \left\langle -\begin{bmatrix}\frac{\partial \mathcal{K}_{ll}}{\partial D} & \frac{\partial \mathcal{M}_{lr}}{\partial D} & 0\\ 0 & \frac{\partial \mathcal{M}_{rr}}{\partial D} & 0\\ \frac{\partial \mathcal{B}_{xl}}{\partial D} & \frac{\partial \mathcal{B}_{xr}}{\partial D} & \frac{\partial \mathcal{B}_{xx}}{\partial D}\end{bmatrix}\begin{Bmatrix}\eta_l\\ \ddot{\eta}_r\\ u_x\end{Bmatrix}_0 + \frac{\partial}{\partial D}\begin{Bmatrix}\mathcal{P}^{0\text{-}g}_{A_{cl}}\\ \mathcal{P}^{0\text{-}g}_{A_{cr}}\\ \mathcal{C}_x\end{Bmatrix}\right\rangle \tag{33}$$

This equation is solved for the sensitivity of the elastic deflection at the nominal cruise condition, and the sensitivities of the aerodynamic loads in the direct structural coordinates are calculated from

$$\frac{\partial\{F^s_A\}}{\partial D} = -[K^a_{ll}]\frac{\partial\{u_l\}}{\partial D} - [K^a_{lx}]\frac{\partial\{u_x\}}{\partial D} + \frac{\partial\{F^s_{A_{C_{0\text{-}g}}}\}}{\partial D}$$

or

$$\frac{\partial\{F^s_A\}}{\partial D} = -[K^a_{ll}][\phi^s_l]\frac{\partial\{\eta_l\}}{\partial D} - [K^a_{lx}]\frac{\partial\{u_x\}}{\partial D} + \frac{\partial\{F^s_{A_{C_{0\text{-}g}}}\}}{\partial D} \tag{34}$$

The inertia load sensitivities are given by

$$\frac{\partial\{F_I\}}{\partial D} = [M][\phi^s_r]\frac{\partial\{\ddot{\eta}_r\}}{\partial D} - \left[\frac{\partial M}{\partial D}\right][\phi^s_r]\{\ddot{\eta}_r\}_0 \tag{35}$$

To avoid expensive eigensolutions, the mode shapes $[\phi^s_r]$ are kept constant and are treated as shape functions. Note that if significant design variables are made, the trim variables are no longer defined in terms of a mean axis. While this by itself will not change the external loads in most cases, it can have an effect on the computed stability derivatives, and the modes must be periodically recalculated to minimize the error.

Sensitivities of Jig Airloads

To compute Eqs. (34) and (35), the sensitivities of the aerodynamic jig shape and the corresponding forces are required, which, in turn, are functions of the nominal cruise loading. For aircraft with high aspect ratio wings, the planform shape and twist that are beneficial for the aerodynamic performance at a given nominal cruise condition tend to have more outboard center of pressure. This feature is undesirable for the maneuver design conditions and leads to heavier structures. Therefore, there appears to be an opportunity for a tradeoff between the 1-g performance and structural loads and weights. To our knowledge, this tradeoff has not yet been fully investigated.

For conditions where the 1-g loading is being optimized, the right-hand side (RHS) of Eq. (23) should be considered to be variable and a function of the structural and aerodynamic design variables, e.g., pretwist. This means that the sensitivity of the RHS should be included in the sensitivity of loads. The first step in computing the jig sensitivity is to compute the sensitivity of the cruise trim state. These sensitivities are given by

$$\frac{\partial}{\partial D}\begin{Bmatrix}\eta_{l_{1\text{-}g}}\\ \ddot{\eta}_{r_{1\text{-}g}}\\ u_{x_{1\text{-}g}}\end{Bmatrix} = \begin{bmatrix}\mathcal{K}_{ll} & \mathcal{M}_{lr} & \mathcal{K}^a_{lx}\\ 0 & \mathcal{M}_{rr} & \mathcal{K}^a_{rx}\\ \mathcal{B}^{1\text{-}g}_{xl} & \mathcal{B}^{1\text{-}g}_{xr} & \mathcal{B}^{1\text{-}g}_{xx}\end{bmatrix}^{-1} \times \left\langle -\begin{bmatrix}\frac{\partial \mathcal{K}_{ll}}{\partial D} & \frac{\partial \mathcal{M}_{lr}}{\partial D} & 0\\ 0 & \frac{\partial \mathcal{M}_{rr}}{\partial D} & 0\\ \frac{\partial \mathcal{B}^{1\text{-}g}_{xl}}{\partial D} & \frac{\partial \mathcal{B}^{1\text{-}g}_{xr}}{\partial D} & \frac{\partial \mathcal{B}^{1\text{-}g}_{xx}}{\partial D}\end{bmatrix}\begin{Bmatrix}\eta_{l_{1\text{-}g}}\\ \ddot{\eta}_{r_{1\text{-}g}}\\ u_{x_{1\text{-}g}}\end{Bmatrix}_0 + \frac{\partial}{\partial D}\begin{Bmatrix}\mathcal{P}^{1\text{-}g}_{A_{cl}}\\ \mathcal{P}^{1\text{-}g}_{A_{cr}}\\ \mathcal{C}^{1\text{-}g}_x\end{Bmatrix}\right\rangle \tag{36}$$

The sensitivities of the jig-shape aerodynamic loads are calculated from

$$\begin{aligned}\frac{\partial\{F^s_{A_{C_{0\text{-}g}}}\}}{\partial D} &= \frac{\bar{q}_{\text{dyn}}}{\bar{q}_{\text{dyn}_{1\text{-}g}}}\frac{\partial\{F^s_{A_{C_{1\text{-}g}}}\}}{\partial D} - \bar{q}_{\text{dyn}}[\text{PPM}_{sa}][\text{AIC}^c]\frac{\partial\{u_{l_{1\text{-}g}}\}}{\partial D}\\ &= \frac{\bar{q}_{\text{dyn}}}{\bar{q}_{\text{dyn}_{1\text{-}g}}}\frac{\partial\{F^s_{A_{C_{1\text{-}g}}}\}}{\partial D} - \bar{q}_{\text{dyn}}[\text{PPM}_{sa}][\text{AIC}^c][\phi^a_l]\frac{\partial\{\eta_{l_{1\text{-}g}}\}}{\partial D}\end{aligned} \tag{37}$$

The sensitivities of the generalized jig aerodynamic loads are given by

$$\begin{aligned}\frac{\partial\{\mathcal{P}^{0\text{-}g}_{A_{C_l}}\}}{\partial D} &= \frac{\bar{q}_{\text{dyn}}}{\bar{q}_{\text{dyn}_{1\text{-}g}}}[\phi^s_l]^T\frac{\partial\{F^s_{A_{C_{1\text{-}g}}}\}}{\partial D} - \bar{q}_{\text{dyn}}[\mathcal{K}^a_{ll}]\frac{\partial\{\eta_{l_{1\text{-}g}}\}}{\partial D}\\ \frac{\partial\{P^{0\text{-}g}_{A_{C_r}}\}}{\partial D} &= \frac{\bar{q}_{\text{dyn}}}{\bar{q}_{\text{dyn}_{1\text{-}g}}}[\phi^s_r]^T\frac{\partial\{F^s_{A_{C_{1\text{-}g}}}\}}{\partial D} - \bar{q}_{\text{dyn}}[\mathcal{K}^a_{rl}]\frac{\partial\{\eta_{l_{1\text{-}g}}\}}{\partial D}\end{aligned} \tag{38}$$

The preceding relationships for the sensitivities of jig loading assume the structural modes are used as the shape function for the aeroelastic analysis, and are kept constant for a particular sensitivity analysis. In the optimization process, the shape functions may be updated to be the current mode shapes of the modified structure at various intervals.

Gust Analysis

AILS aeroservoelastic gust load capabilities include 1) random frequency response analysis for displacement, velocity, acceleration, loads, and stress; 2) rms and covariance (phased random response) calculations for all of the preceding items; 3) flight control and active load alleviation system; and 4) analytical sensitivities of gust response to structural design variables and control gains. The gust response analysis is also formulated in modal coordinates and a linear frequency domain approach is used. In the solution of random gust loads, first the frequency-response function of the aircraft traveling through a sinusoidal gust of unit amplitude is calculated. The general equation of motion for the aircraft response to a si-

nusoidal gust and pilot input of the same frequency is given as

$$\begin{bmatrix} (1+ig)\mathcal{H}_{ll} + \mathcal{H}^a_{ll} & \mathcal{H}^a_{lr} & \mathcal{H}^a_{lc} & 0 \\ \mathcal{H}^a_{rl} & \mathcal{H}^a_{rr} & \mathcal{H}^a_{rc} & 0 \\ \mathcal{H}^a_{cl} & \mathcal{H}^a_{cr} & \mathcal{H}^a_{cc} & 0 \\ 0 & 0 & 0 & 0 \end{bmatrix} \begin{Bmatrix} \eta_l \\ \eta_r \\ \eta_c \\ u_x \end{Bmatrix} + (i\omega)^2 \begin{bmatrix} \mathcal{M}_{ll} & \mathcal{M}_{lr} & \mathcal{M}_{lc} & 0 \\ \mathcal{M}_{rl} & \mathcal{M}_{rr} & \mathcal{M}_{rc} & 0 \\ \mathcal{M}_{cl} & \mathcal{M}_{cr} & \mathcal{M}_{cc} & 0 \\ 0 & 0 & 0 & 0 \end{bmatrix} \begin{Bmatrix} \eta_l \\ \eta_r \\ \eta_c \\ u_x \end{Bmatrix} + \begin{bmatrix} 0 & 0 & 0 & 0 \\ 0 & 0 & 0 & 0 \\ 0 & 0 & (1+ig)\mathcal{H}_{xx} & -(1+ig)\mathcal{H}_{xx} \\ \mathcal{B}_{xl} & \mathcal{B}_{xr} & \mathcal{B}_{xc} & \mathcal{B}_{xx} \end{bmatrix} \begin{Bmatrix} \eta_l \\ \eta_r \\ \eta_c \\ u_x \end{Bmatrix} = \bar{q}_{\text{dyn}} \frac{U_g(i\omega)}{V_\infty} \begin{Bmatrix} \mathcal{F}^g_l \\ \mathcal{F}^g_r \\ \mathcal{F}^g_c \\ 0 \end{Bmatrix} + \begin{Bmatrix} 0 \\ 0 \\ 0 \\ F_{\text{pilot}}(i\omega) \end{Bmatrix} \tag{39}$$

where the implicit dependence of the aerodynamic terms on frequency is omitted for brevity. Equation (39) can be rewritten in a symbolic form as

$$[A(i\omega)] \begin{Bmatrix} \eta_l(i\omega) \\ \eta_r(i\omega) \\ \eta_c(i\omega) \\ u_x(i\omega) \end{Bmatrix} = \bar{q}_{\text{dyn}} \frac{U_g(i\omega)}{V_\infty} \begin{Bmatrix} F^g_l(ik) \\ F^g_r(ik) \\ F^g_c(ik) \\ 0 \end{Bmatrix} + \begin{Bmatrix} 0 \\ 0 \\ 0 \\ F_{\text{pilot}}(i\omega) \end{Bmatrix} \tag{40}$$

where

$$[A(i\omega)] = \begin{bmatrix} (1+ig)\mathcal{H}_{ll} + \mathcal{H}^a_{ll} - \omega^2\mathcal{M}_{ll} & \mathcal{H}^a_{lr} - \omega^2\mathcal{M}_{lr} & \mathcal{H}^a_{lc} - \omega^2\mathcal{M}_{lc} & 0 \\ \mathcal{H}^a_{rl} - \omega^2\mathcal{M}_{rl} & \mathcal{H}^a_{rr} - \omega^2\mathcal{M}_{rr} & \mathcal{H}^a_{rc} - \omega^2\mathcal{M}_{rc} & 0 \\ \mathcal{H}^a_{cl} - \omega^2\mathcal{M}_{cl} & \mathcal{H}^a_{cr} - \omega^2\mathcal{M}_{cr} & \mathcal{H}^a_{cc} + (1+ig)\mathcal{H}_{xx} - \omega^2\mathcal{M}_{cc} & -(1+ig)\mathcal{H}_{xx} \\ \mathcal{B}_{xl} & \mathcal{B}_{xr} & \mathcal{B}_{xc} & \mathcal{B}_{xx} \end{bmatrix} \tag{41}$$

Note that different points on the aircraft experience the same sinusoidal velocity profile with time delays proportional to the longitudinal distance from a reference point (X_0/V_∞). The normalized elastic modes, $[\phi_l]$, used in the aeroservoelastic analysis, are with the control-surface actuators assumed in the locked position. The elastic modes are augmented with the rigid modes of the control surface, $[\phi_c]$.

The displacement frequency response is obtained from

$$\begin{Bmatrix} \eta_l(i\omega) \\ \eta_r(i\omega) \\ \eta_c(i\omega) \\ u_x(i\omega) \end{Bmatrix} = [A(i\omega)]^{-1} \left(\bar{q}_{\text{dyn}} \frac{U_g(i\omega)}{V_\infty} \begin{Bmatrix} \mathcal{F}^g_l(i\omega) \\ \mathcal{F}^g_r(i\omega) \\ \mathcal{F}^g_c(i\omega) \\ 0 \end{Bmatrix} + \begin{Bmatrix} 0 \\ 0 \\ 0 \\ F_{\text{pilot}}(i\omega) \end{Bmatrix} \right) \tag{42}$$

In calculating the frequency response function to the sinusoidal gust, the pilot input is set to zero, and U_g is unity. The direct acceleration, aerodynamic, and inertia loads in the frequency domain are calculated from the modal response. The expressions for aerodynamic and inertia loads are

$$\{F^s_A(i\omega)\} = -[K^a(ik)][\phi_l \ \phi_r \ \phi_c] \begin{Bmatrix} \eta_l(i\omega) \\ \eta_r(i\omega) \\ \eta_c(i\omega) \end{Bmatrix} \tag{43}$$

$$\{F^s_I(i\omega)\} = \omega^2[M][\phi_l \ \phi_r \ \phi_c] \begin{Bmatrix} \eta_l(i\omega) \\ \eta_r(i\omega) \\ \eta_c(i\omega) \end{Bmatrix} \tag{44}$$

where

$$[K^a(ik)] = -\bar{q}_{\text{dyn}}[\text{PPM}_{sa}][\text{AIC}^c(ik)][\text{SPM}_{as}] \tag{45}$$

In general, the frequency domain solution for all response quantities can be cast in the following general form:

$$\{y(i\omega)\} = [H_g(i\omega)]U_g(i\omega) + [B(i\omega)]F_{\text{pilot}}(i\omega) \tag{46}$$

For example, the response matrix for the aerodynamic loads in the direct structural coordinates can be derived from Eqs. (42) and (43):

$$[H_g(i\omega)]_{\text{aeroloads}} = -\frac{\bar{q}_{\text{dyn}}}{V_\infty}[K^a(ik)][\phi^a_l \ \phi^a_r \ \phi^a_c \ 0][A(i\omega)]^{-1} \begin{Bmatrix} F^g_l(i\omega) \\ F^g_r(i\omega) \\ F^g_c(i\omega) \\ 0 \end{Bmatrix} \tag{47}$$

The power spectral density (PSD) of the ith element of $\{y\}$ is related to the PSD of the gust velocity by

$$\phi_{y_i}(\omega) = |H_{g_i}(\omega)|^2 \phi_g(i\omega) \tag{48}$$

The gust PSD is computed using the von Kármán and Dryden PSD functions. The variance and covariance of the response quantities are determined from

$$\begin{aligned} \text{cov}(y_i, y_j) &= \frac{1}{2}\int_0^\infty [y_i(\omega)y^*_j(\omega) + y^*_i(\omega)y_j(\omega)]\, d\omega \\ &= \frac{1}{2}\int_0^\infty [H_{g_i}(\omega)H^*_{g_j}(\omega) + H^*_{g_i}(\omega)H_{g_j}(\omega)]\phi^2_g(\omega)\, d\omega \end{aligned} \tag{49}$$

The correlated loads as well as their rms values are determined using the square foot of Eq. (49). The number of positive-slope zero crossings, N_0, is given by

$$N_0|_{y_i} = \frac{1}{2\pi}\sqrt{\frac{\int_0^\infty \omega^2 H_{g_i}(\omega)H^*_{g_i}(\omega)\phi^2_g(\omega)\, d\omega}{\int_0^\infty H_{g_i}(\omega)H^*_{g_i}(\omega)\phi^2_g(\omega)\, d\omega}} \tag{50}$$

The sensitivity of the frequency-domain modal displacement vector with respect to the structural and control design variables are calculated from

$$\frac{\partial}{\partial D}\begin{Bmatrix} \eta_l(i\omega) \\ \eta_r(i\omega) \\ \eta_c(i\omega) \\ u_x(i\omega) \end{Bmatrix} = -[A(i\omega)]^{-1}\frac{\partial[A(i\omega)]}{\partial D}[A(i\omega)]\begin{Bmatrix} \eta_l(i\omega) \\ \eta_r(i\omega) \\ \eta_c(i\omega) \\ u_x(i\omega) \end{Bmatrix}_0 \tag{51}$$

The sensitivity of the frequency-domain loads is predicted in a similar fashion, and the sensitivity of the covariance between different response quantities is determined from

$$\frac{\partial\, \text{cov}(y_i, y_j)}{\partial D} = \frac{1}{2}\int_0^\infty \left[H_{g_i}(\omega)\frac{\partial H^*_{g_j}(\omega)}{\partial D} + \frac{\partial H_{g_i}(\omega)}{\partial D}H^*_{g_j}(\omega) + H_{g_j}(\omega)\frac{\partial H^*_{g_i}(\omega)}{\partial D} + \frac{\partial H_{g_j}(\omega)}{\partial D}H^*_{g_i}(\omega)\right]\phi^2_g(\omega)\, d\omega \tag{52}$$

Results

The static and dynamic results for AILS are compared with a proprietary program (C4EZ)[16] and MSC/NASTRAN.[17] AILS capabilities are demonstrated for two types of aircraft: one is a wide-body subsonic transport and the other is an early HSCT configuration. A subset of the results are presented next for the subsonic flight regime of both aircraft.

Static Maneuver Loads—Subsonic Transport

Figure 3 shows the structural model of a wide-body transport aircraft. The structural model consists of beam representations of the wing, fuselage, horizontal, and vertical tails. This aircraft was modeled in ADOP/AILS, MSC/NASTRAN, and C4EZ. Comparisons of frequencies and mode shapes among the NASTRAN, ADOP/AILS, and D7QB (an in-house modal analysis program) have been made, and the modes and frequencies calculated by the three programs (not presented here) were in very close agreement.

The lifting surface model of this aircraft (doublet lattice) is shown in Fig. 4. MSC/NASTRAN uses an earlier version of the doublet-lattice code, which is somewhat different in the treatment of fuselage than the currently used proprietary version. For this reason, the fuselage aerodynamic was not mod-

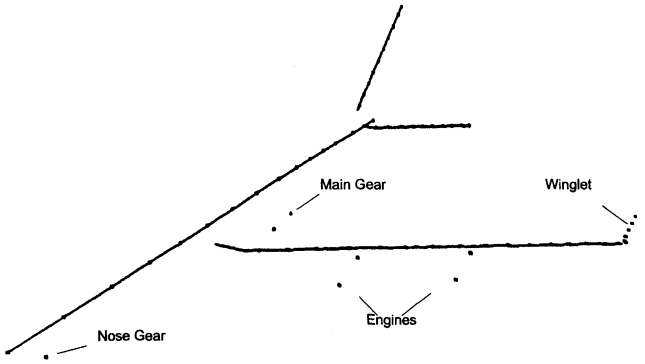

Fig. 3 Structural FEM for a wide-body subsonic transport aircraft test case.

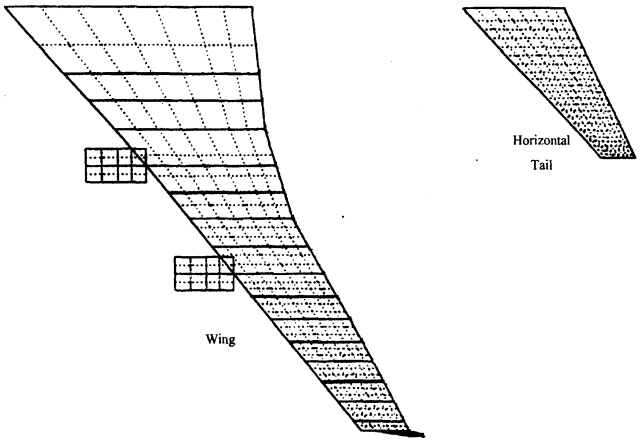

Fig. 4 Aerodynamic lifting surface model for a wide-body subsonic transport. (Fuselage is not modeled to compare with MSC/NASTRAN.)

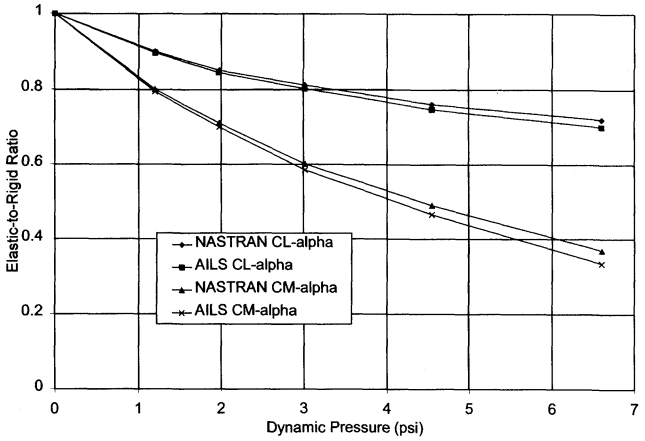

Fig. 5 Comparison between AILS and NASTRAN lift and moment coefficients *E/R* for subsonic transport test case at Mach 0.8.

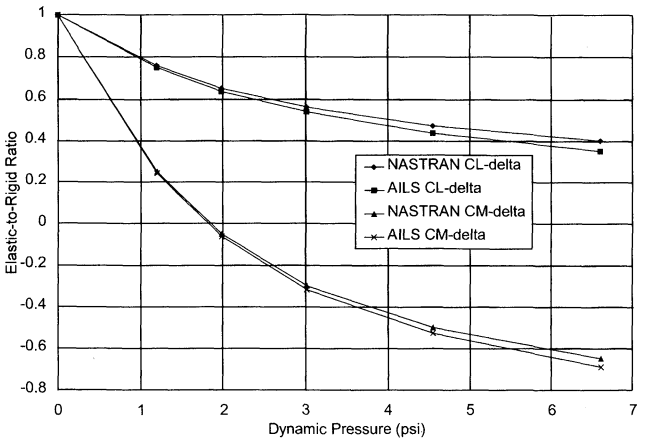

Fig. 6 Comparison between AILS and NASTRAN full aircraft aileron *E/R* for subsonic transport case at Mach 0.8.

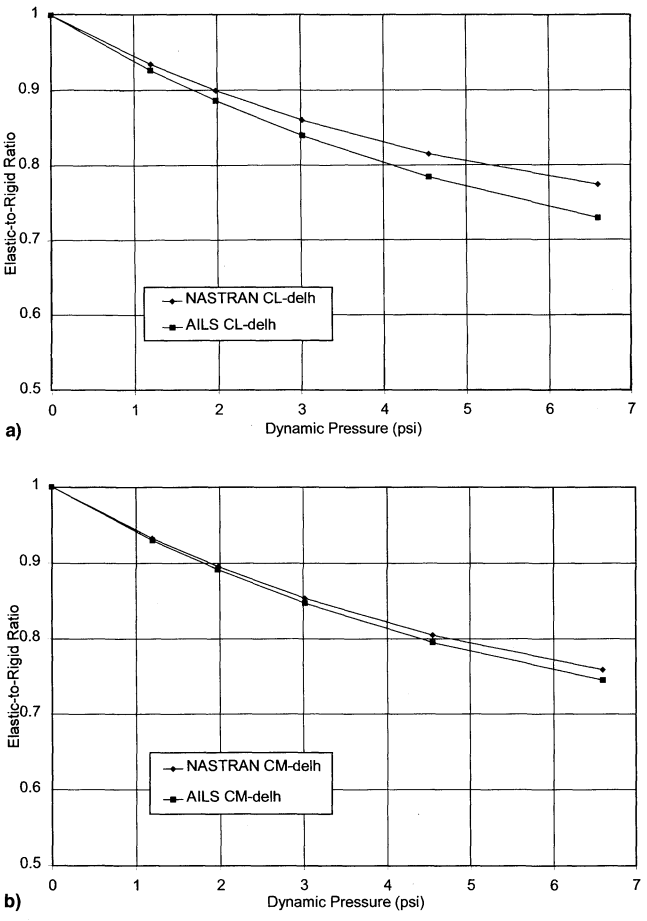

Fig. 7 Comparison between AILS and NASTRAN a) lift and b) moment coefficient caused by horizontal tail *E/R* for subsonic transport case (full aircraft, Mach 0.8).

eled in both representations (ADOP/AILS and MSC/NASTRAN).

Figure 5 shows the comparison of NASTRAN and AILS elastic-to-rigid ratios (E/R) for the full aircraft lift and moment coefficient derivatives with respect to the angle of attack at Mach 0.8. The results demonstrate a very good agreement between AILS and NASTRAN. It should be emphasized that MSC/NASTRAN uses a direct approach and AILS uses a modal approach.

The comparison for the symmetric aileron derivative E/R for lift and pitch moment coefficients (Fig. 6) indicates a good agreement between the two methodologies. Note that the E/R of incremental lift caused by symmetric aileron becomes negative for dynamic pressure above 2.0 psi.

In Fig. 7a, horizontal tail lift derivative E/R from AILS is compared with MSC/NASTRAN results. The comparison is marginal because of the small number of aft fuselage modes to satisfactorily represent the aft fuselage bending. While a methodology has been devised to reduce this difference significantly, it is beyond the scope of this paper. The AILS results for the E/R of the aircraft pitching moment derivative to the horizontal tail angle is compared with MSC/NASTRAN results in Fig. 7b. The comparison is better than lift derivative.

The verification of AILS' static aeroelastic loads procedure will be discussed next. Figure 8 shows results of distributed shear loads along the span for the subsonic transport test case at Mach 0.8 and 30,000 ft performing a positive 2.5-g pull-up maneuver. The airplane is fully trimmed using angle of attack and horizontal tail deflection as trim variables. The AILS loads results compare very well with MSC/NASTRAN.

Figure 9 shows the integrated wing bending moment (combined aerodynamic and inertia) across the span of the wing for a condition in which the angle of attack is specified to be 5.73 deg, and the vertical acceleration and horizontal tail deflection are treated as trim variables. The results between AILS and NASTRAN are virtually indistinguishable.

Figure 10 shows the results of the modal convergence for the tip deflection, root bending moment, E/R of $C_{L\alpha}$, and $C_{M\alpha}$, and their difference with MSC/NASTRAN. The root bending moment calculated from the AILS modal approach when compared with the NASTRAN direct method is within 2% with 20 modes, within less than 1% with 30 modes, and indistinguishable with 40 modes. As the number of modes increases, all of the response quantities tend to converge to within less than 3% of the direct approach.

Figure 11 shows the lift on individual aerodynamic bays caused by only the elastic deflections for 10, 30, and 50 modes. These results are for the subsonic transport test case performing a 2.5-g pull-up flying at 30,000 ft and Mach 0.8. While the results for 10 modes are poor, they seem to have converged at 30 modes, and using 50 modes causes insignificant changes in the results.

Figure 12 shows the displacement differences between the modal and direct solutions at the same flight condition discussed in the preceding text. The maximum errors in displacement and rotation are 6.68 in. at the fuselage nose, and 0.011 rad at the horizontal tail. The maximum deflection at the wing

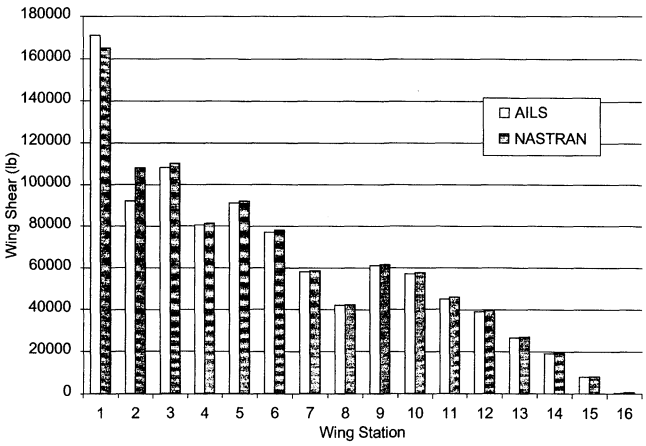

Fig. 8 Integrated vertical shear (combined aerodynamic and inertia) for the subsonic transport test case (2.5-g pull-up at Mach 0.8, q_{dyn} = 1.959 psi).

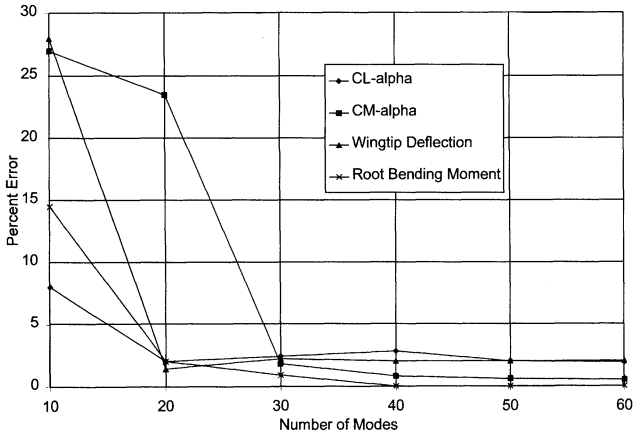

Fig. 10 Convergence of AILS solutions with increasing number of modes (α = 5.73 deg, Mach 0.8, q_{dyn} = 6.583 psi).

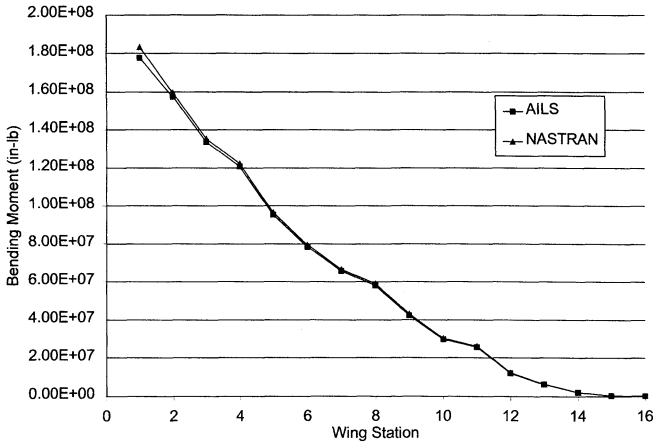

Fig. 9 Integrated out-of-plane bending moment (combined aerodynamic and inertia) for the subsonic transport test case (α = 5.73 deg at Mach 0.8, q_{dyn} = 6.583 psi).

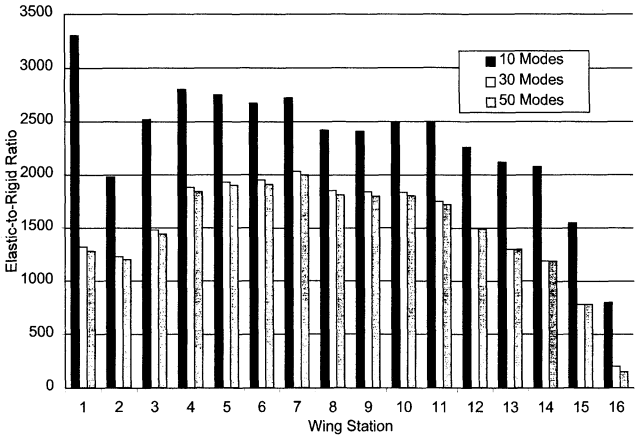

Fig. 11 Lift distribution caused by elastic deflection for varying numbers of modes. Subsonic transport in a 2.5-g pull-up at Mach 0.8, q_{dyn} = 1.959 psi.

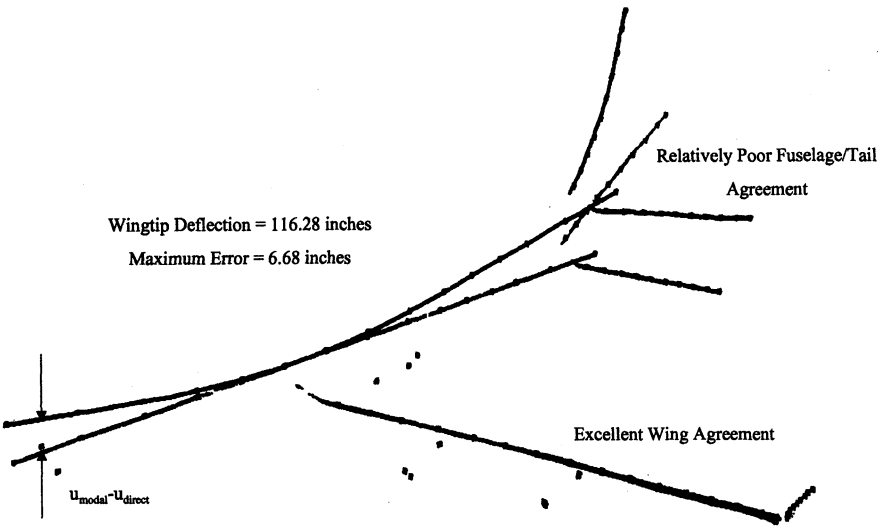

Fig. 12 Differences in deflections calculated with the modal and direct solutions for the wide-body subsonic transport test case (Mach 0.8, sea level, 5.73 deg α).

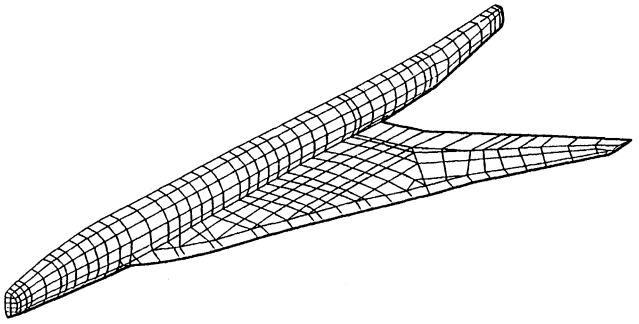

Fig. 13 FEM of the HSCT aircraft test case.

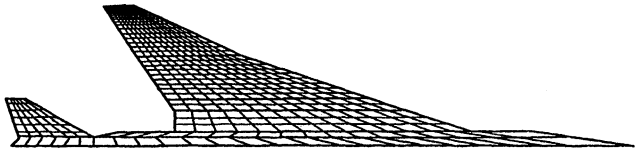

Fig. 14 Lifting surface model for HSCT aircraft test case.

tip is 116.28 in. Note that wing displacements are very accurately captured using the modal approach.

Static Maneuver Loads—HSCT

AILS static aeroelastic analysis was also applied to an earlier version of an HSCT configuration designed for a supersonic cruise of Mach 2.2. This model is used as a test case only. Figures 13 and 14 show the structural finite element and aerodynamic doublet-lattice models used in this study.

The aeroelastic restrained and unrestrained lift and moment curve slopes for the full aircraft are shown in Figs. 15a and 15b, respectively. The comparison of AILS derivatives with MSC/NASTRAN results reveals moderate discrepancies in the restrained derivatives at high dynamic pressures. This discrepancy is attributed to the support methodology in the direct solution method. Although both solutions are for free-flying aircraft, the direct method of aeroelastic solution requires supporting the aircraft at some FEM node point. Although the direct aeroelastic loads are balanced, any small numerically unbalance loads will cause significant local deformation at the support point if it is relatively flexible. This issue is not relevant to the modal aeroelastic analysis such as AILS.

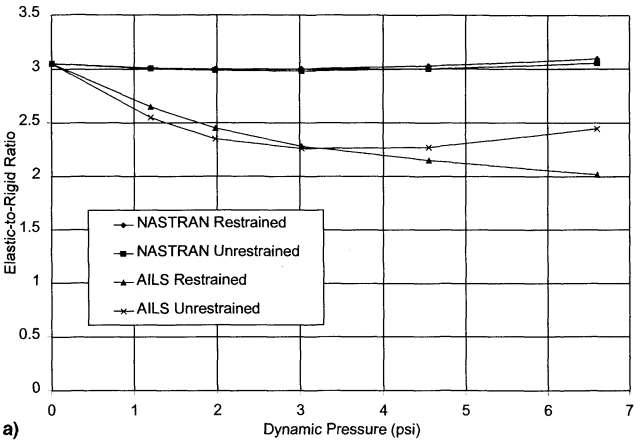

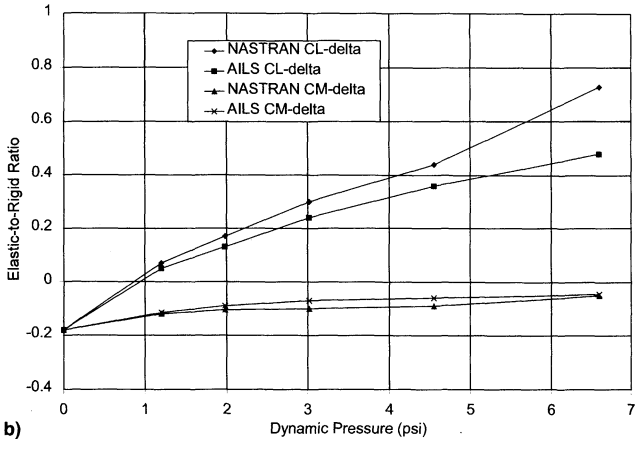

Fig. 15 AILS vs NASTRAN elastic a) $C_{L\alpha}$ and b) $C_{M\alpha}$ comparison for an HSCT aircraft at Mach 0.8.

Figure 16 compares the elastic wing-tip deflections for HSCT in a 2.5-g pull-up maneuver at Mach 0.8 between AILS and MSC/NASTRAN as a function of dynamic pressure. The correlation is excellent between the two sets of results at all dynamic pressure values.

A comparison between AILS and MSC/NASTRAN distributed pressure results (not presented here) was also made, and the results are indistinguishable.

Static Maneuver Load Sensitivities

AILS analytical sensitivities of free-flying aircraft loads are verified against numerical (finite difference) sensitivities. Figure 17 shows the analytical sensitivity of the wing out-of-plane bending-moments (balanced, free-flying full aircraft) to the out-of-plane bending moment of inertia of the root of the wing. A comparison with a finite difference estimate of the derivative shows good agreement.

Random Gust Loads

Figure 18 shows the frequency response caused by a 99-ft/s random gust with von Kármán spectrum. In this figure, the wing-tip acceleration PSD calculated by AILS and C4EZ are shown on a linear scale. These results agree well up to 3.5 Hz. The difference in higher-frequency responses are a result of the differences in the higher eigenvalues and modes caused by the more accurate eigensolution in ADOP. The rms values for the tip vertical acceleration per unit gust are 56.125 $(\text{in./s}^2)/(\text{ft/s})$ for the AILS solution, and 56.045 $(\text{in./s}^2)/(\text{ft/s})$ for the C4EZ solution. The discrepancies in higher modes amount to a difference of 0.14% in the rms values, which is negligible.

Figure 19 shows the validation of an AILS gust system for a system with automatic flight control. The results in this figure include an active feedback system that ties the symmetric aileron deflection to the wing-tip-measured accelerations. Again, the results of the AILS for the subsonic aircraft are very close to C4EZ.

Figure 20 shows that the wing root vertical shear power spectrum, as calculated by the AILS, correlates well with the C4EZ's results for the subsonic transport aircraft test case.

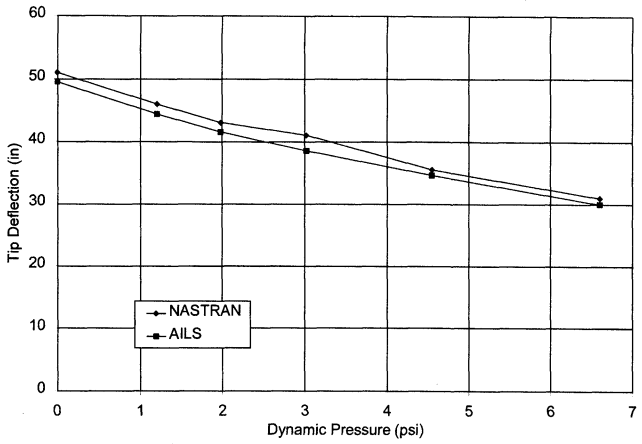

Fig. 16 Comparison of AILS and NASTRAN wing-tip deflection for the HSCT test case (2.5-*g* pull-up at Mach 0.8).

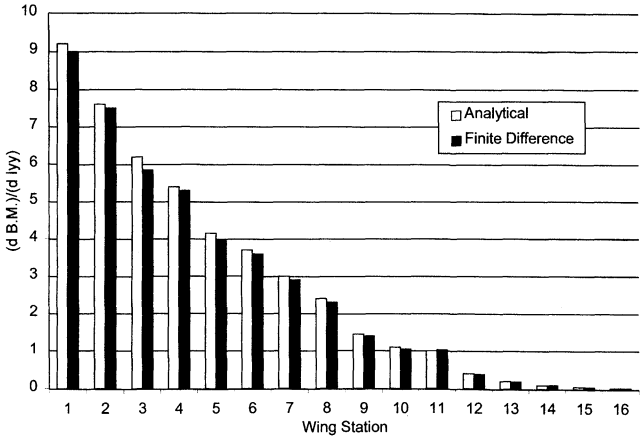

Fig. 17 Sensitivity of wing bending moments to bending stiffness of the root element of the subsonic transport test case.

PSD Gust Load Sensitivities

The validation of the sensitivity to the control gain variables is done through comparison with a numerical finite difference approach. The sensitivity of the wing-tip vertical displacement frequency response to the gain of an active control system linking the wing-tip acceleration to the symmetric aileron motion are shown in Fig. 21. Figure 21 shows that the numerical and analytical sensitivities are indistinguishable.

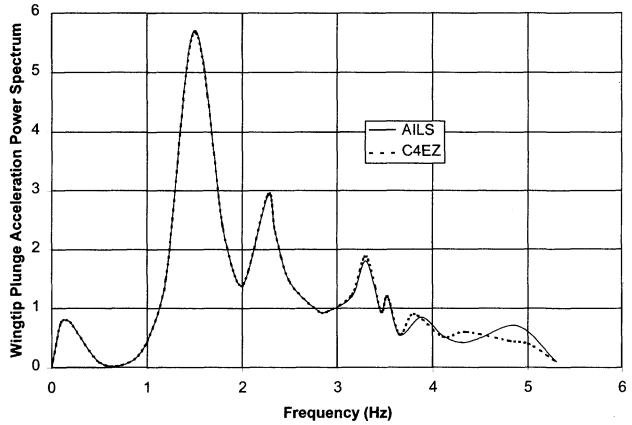

Fig. 18 Verification of AILS gust response calculation for subsonic transport: wing-tip plunge acceleration power spectrum (Mach 0.4, q_{dyn} = 1.64 psi, gust velocity = 99 ft/s).

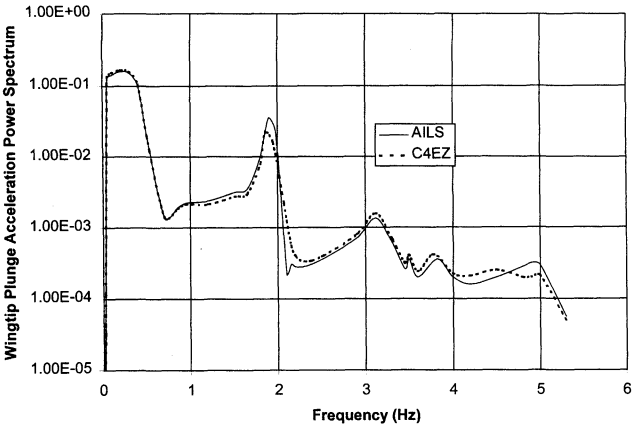

Fig. 19 Verification of AILS gust response calculation with automatic flight control system: wing-tip plunge acceleration power spectrum.

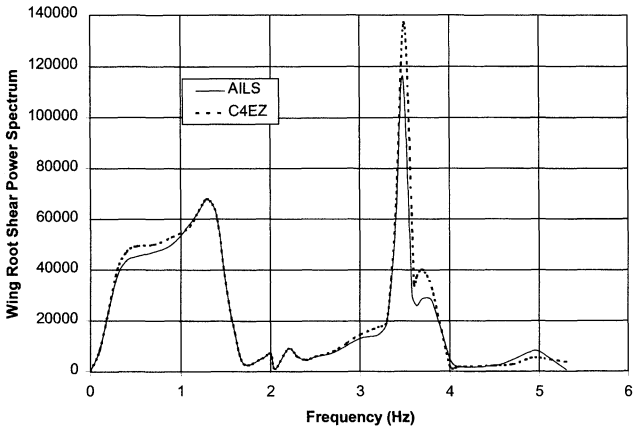

Fig. 20 Verification of AILS gust response calculation for subsonic transport: wing root shear power spectrum (Mach 0.4, q_{dyn} = 1.64 psi, gust velocity = 99 ft/s).

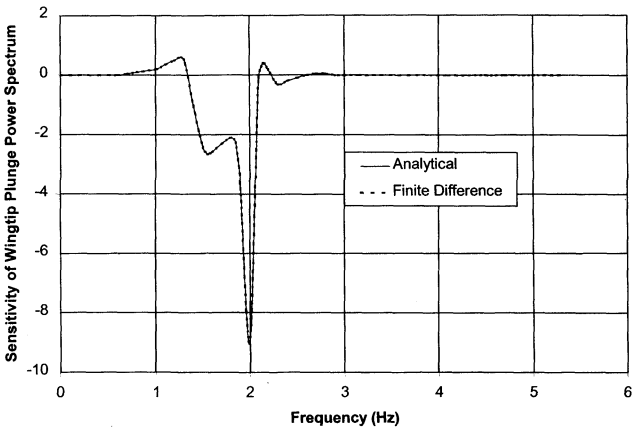

Fig. 21 Verification of AILS analytical gust response senstivities to control-system parameters (Mach 0.4, q_{dyn} = 1.64, psi, gust velocity = 99 ft/s).

Conclusions

A first release of an AILS has been developed as part of a large-scale ADOP. This allows the optimization process to include the effects of load sensitivities and to take full advantage of passive and active load alleviation. AILS capabilities include linear steady maneuver and PSD gust analysis. AILS load analyses have been verified against C4EZ and MSC/NASTRAN using two advanced-design transport aircraft models. AILS analytical load sensitivities for steady maneuver and gust are verified using a numerical finite difference approach. ADOP/AILS will provide a useful tool for the design of modern aircraft with advanced materials and active control systems.

References

[1]D'Vari, R., and Baker, M. L., "A Static and Dynamic Aeroelastic Loads and Sensitivity Analysis for Structural Loads Optimization and Its Application to Transport Aircraft," AIAA Paper 93-1643, April 1993.

[2]Albano, E., and Rodden, W. P., "A Doublet Lattice Method for Calculating Lift Distributions on Oscillating Surfaces in Subsonic Flow," *AIAA Journal*, Vol. 7, No. 2, 1969, pp. 279–285; also Vol. 7, No. 11, 1969, p. 2192.

[3]Giesing, J. P., Kalman, T. P., and Rodden, W. P., "Subsonic Unsteady Aerodynamics for General Configurations," *Application of the Doublet Lattice Method and the Method of Images to Lifting Surface/Body Interference*, Pt. II, Vol. I, U.S. Air Force Flight Dynamics Lab., Rept. AFFDL-TR-71-5, April 1972.

[4]Dodd, A. J., Kadrinka, K. E., Loikkanen, M. J., Rommel, B. A., Sikes, G. D., Strong, R. C., and Tzong, T. J., "Aeroelastic Design Optimization Program," *Journal of Aircraft*, Vol. 27, No. 12, 1990, pp. 1028–1036.

[5]Tzong, T. J., Sikes, G. D., and Loikkanen, M. J., "Multidisciplinary Design Optimization of a Large Transport Aircraft Wing," AIAA Paper 92-1002, Feb. 1992.

[6]Vanderplaats, G. N., *DOT User's Manual*, Version 2.04b, Engineering Design Optimization, Inc., Santa Barbara, CA, 1989.

[7]D'Vari, R., Hoffman, K., and Tran, T., "Aeroelastic Maneuver Loads and Structural Optimization for High Speed Civil Transport (HSCT) Aircraft," AIAA Paper 92-2398, April 1992.

[8]Sikes, G., Tzong, G., and Sharma, A., "Flutter Optimization of Large Transport Aircraft," AIAA Paper 92-4795, Sept. 1992.

[9]Chen, P. C., and Liu, D. D., "A Harmonic Gradient Method for Unsteady Airloads Analysis," *Journal of Aircraft*, Vol. 24, No. 9, 1987, pp. 696–702.

[10]Chen, P. C., and Liu, D. D., "Unsteady Supersonic Computations of Arbitrary Wing-Body Configurations Including External Stores," *Journal of Aircraft*, Vol. 27, No. 2, 1990, pp. 108–116.

[11]Woodward, F. A., "An Improved Method for the Aerodynamic Analysis of Wing-Body-Tail Configurations in Subsonic and Supersonic Flow, Part I—Theory and Applications," NASA CR-2228, May 1973.

[12]Pitt, D. M., and Eversman, W., "Development and Application of the Subsonic and Supersonic Doublet Point Method," *AIAA/ASME/ASCE/AHS/ASC 29th Structures, Structural Dynamics, and Materials Conference*, Williamsburg, VA, April 1988.

[13]Baker, M. L., "CFD Based Corrections for Linear Aerodynamic Methods," *Numerical Unsteady Aerodynamic and Aeroelastic Simulation*, AGARD 822, March 1998.

[14]Baker, M. L., Goggin, P. J., and Yuan, K. A., "Calculations of Corrections to Linear Aerodynamic Methods for Static and Dynamic Analysis and Design," AIAA Paper 98-2072, April 1998.

[15]Harder, R. L., and Desmarais, R. N., "Interpolation Using Surface Splines," *Journal of Aircraft*, Vol. 9, No. 2, 1972, pp. 189–191.

[16]McGrew, J. A., "Flutter and Dynamic Response Analysis Program—C4EZ," Vols. I–II, McDonnell Douglas, Rept. J6469, Long Beach, CA, June 1978.

[17]Rodden, W. P., and Johnson, E. H., "MSC/NASTRAN Handbook for Aeroelastic Analysis, Version 68," MacNeal-Schwendler Corp., Pasadena, CA, 1994.